SF2A 2011
G. Alecian, K. Belkacem, R. Samadi and D. Valls-Gabaud (eds)

MODELING THE POLARIZATION OF RADIO-QUIET AGN: FROM THE OPTICAL TO THE X-RAY BAND

F. Marin[1] and R. W. Goosmann[1]

Abstract. A thermal active galactic nucleus (AGN) consist of a powerful, broad-band continuum source that is surrounded by several reprocessing media with different geometries and compositions. Here we investigate the expected spectropolarimetric signatures in the optical/UV and X-ray wavebands as they arise from the complex radiative coupling between different, axis-symmetric AGN media. Using the latest version of the Monte-Carlo radiative transfer code STOKES, we obtain spectral fluxes, polarization percentages, and polarization position angles. In the optical/UV, we assume unpolarized photons coming from a compact source that are reprocessed by an optically-thick, dusty torus and by equatorial and polar electron-scattering regions. In the X-ray band, we additionally assume a lamp-post geometry with an X-ray source irradiating the accretion disk from above. We compare our results for the two wavebands and thereby provide predictions for future X-ray polarimetric missions. These predictions can be based on present-day optical/UV spectropolarimetric observations. In particular, we conclude that the observed polarization dichotomy in the optical/UV band should extend into the X-ray range.

Keywords: galaxies: active - galaxies: Seyfert - polarization - radiative transfer

1 Introduction

Since the early observations by Fath (1909), active galactic nuclei (AGN) have been intensively observed at all possible wavelengths using ground-based and space telescopes. The core of an AGN cannot be resolved by current optical instruments. In addition to that we find that in type-2 objects (those with narrow optical emission lines) the central engine is hidden by optically thick dust blocking most of the light. According to the unified scheme of AGN (Antonucci 1993), the obscuring dust is distributed anisotropically and in type-1 AGN, which show broad optical emission lines, the central region is directly visible. This anisotropic distribution of absorbing and scattering media in AGN must induce a net polarization that we can exploit in order to investigate the complex radiative coupling between the innermost components of AGN. In fact, spectropolarimetry is a unique tool to probe the unresolvable parts of AGN thanks to two more independent observables it adds: the percentage and the position angle of polarization. So far, spectropolarimetry observations could be performed from the radio to the optical/UV band, but with the launch of the GEMS satellite (Kallman et al. 2010) the first X-ray polarization data of bright AGN is soon going to be in reach.

To interpret the data, polarization modeling of the radiative interplay between different AGN components is necessary. Such modeling has been conducted previously by a number of authors (see e.g. Kartje 1995; Smith et al. 2004; Wolf & Henning 1999; Goosmann & Matt 2011). For computational reasons, some models are restricted to a single-scattering approach following the suggestion by Henney & Axon (1995) about the predominance of first-order scattering in optically thick media. But one should bear in mind that this argument does not necessarily hold for the multiple scattering between several non-absorbing, electron-scattering components. Also, previous modeling is most often limited to a given waveband.

In this research note, we present a composite, multiple-scattering and reprocessing model of AGN from which spectropolarimetric fluxes are computed simultaneously in the optical/UV and in the X-ray band. Our model setup is based on the classical, axis-symmetric unified scheme of AGN (Urry & Padovani 1995) and we are particularly interested in the polarization properties as a function of wavelength and viewing direction.

[1] Observatoire astronomique de Strasbourg, Section Hautes Energies, 11 Rue de l'Université, 67000 Strasbourg, France

irradiated accretion disk	flared disk	dusty torus	polar outflows
(only present for X-rays)	$R_{\rm min} = 0.02$ pc	$R_{\rm min} = 0.1$ pc	$R_{\rm min} = 0.3$ pc
$R_{\rm disk} = 0.0004$ pc	$R_{\rm max} = 0.04$ pc	$R_{\rm max} = 0.5$ pc	$R_{\rm max} = 1.8$ pc
$h_{\rm disk} = 3.25 \times 10^{-7}$ pc	half-opening angle = 20°	half-opening angle = 60°	half-opening angle = 40°
vertical optical depth >600	equat. optical depth = 1	equat. optical depth = 750	vertical optical depth = 0.03
neutral reprocessing	electron scattering	Mie scattering/neutral reprocessing	electron scattering

Table 1. Parameters of the different model components. The accretion disk is only present when modeling the X-ray range. The elevated primary X-ray source is located on the disk axis and subtends a half-angle of 76° with the disk. Note that for the polar outflow, the half-opening angle is measured with respect to the vertical, symmetry axis of the torus, while for the flared-disk the half-opening angle is taken with respect to the equatorial plane.

When observing the optical polarization of AGN, a dichotomy is found for the polarization angle (Antonucci 1983): at type-2 viewing angles, the position angle of the polarization is most often directed perpendicularly to the central radio structure; at type-1 viewing angles, the polarization vector favors a direction that is aligned with the (projected) radio axis. Assuming that the radio structure is stretched along the symmetry axis of the torus, our modeling allows us to test if we can reproduce this observed dichotomy. In the following, we define *parallel* (or *perpendicular*) polarization according to the preferentially observed polarization angle of *type-1* (or *type-2*) AGN. When plotting our results, we distinguish parallel polarization by adding a negative sign to the polarization percentage.

2 Modeling the unified scheme of AGN

2.1 Model setup for the AGN structure

We investigate the radiative coupling between different axis-symmetric emission and reprocessing regions: the inner and outer parts of the accretion disk, the obscuring equatorial dust region, and double-conical outflows along the polar direction.

We consider a compact continuum source of unpolarized photons being emitted isotropically according to a power-law $F_\nu \propto \nu^{-\alpha}$ with index $\alpha = 1$. For the optical/UV part (1600 Å – 8000 Å) we assume the continuum source to be very compact and quasi point-like. For the X-ray range (1 keV – 100 keV), we adopt a lamp-post geometry and include X-ray reprocessing of the primary radiation by the underlying disk. The primary source is located at low height on the disk axis subtending a large solid angle with the disk.

The source region is surrounded by a geometrically and optically thin scattering annulus with a flared shape. This radiation-supported wedge plays a major role as it produces a parallel polarization signature in type-1 view by electron scattering (see e.g. Chandrasekhar 1960, Angel 1969, Antonucci 1984, Sunyaev & Titarchuk 1985). At larger radius an optically thick, elliptical dusty torus surrounds the system. It shares the same symmetry plane as the flared disk and is responsible for the optical obscuration at type-2 views. The torus funnel supposedly collimates a mildly-ionized, optically thin outflow stretched along the symmetry axis of the system. The polar wind has an hourglass shape and is centered on the photon source. Parameters defining the shape and the composition of the three/four reprocessing regions are summarized in Table 1. The dust model used for the torus at optical/UV wavelengths is based on a prescription for Galactic dust as described in Goosmann & Gaskell (2007). In the X-ray band, we assume neutral reprocessing for the torus and for the accretion disk. Details of this reprocessing model can be found in Goosmann & Matt (2011).

2.2 The radiative transfer code STOKES

We apply the latest version of the Monte-Carlo code STOKES (`www.stokes-program.info`). For details on the code, consult Goosmann & Gaskell (2007) and Goosmann & Matt (2011). It conducts radiative transfer in complex emission and reprocessing environments and includes the treatment of polarization. The calculations include multiple scattering, an angle-dependent analysis in 3D, and different dust models. The STOKES code computes the total flux spectrum, the polarization angle, the percentage of polarization, and the polarized flux. The reprocessing physics depends on the energy band considered. Electron and Mie scattering are assumed in the optical/UV waveband; Compton scattering and neutral reprocessing predominate in the X-ray range.

We compute the spectropolarimetric flux as a function of wavelength or photon energy at a given polar viewing angle, i, that is measured with respect to the symmetry axis of the system.

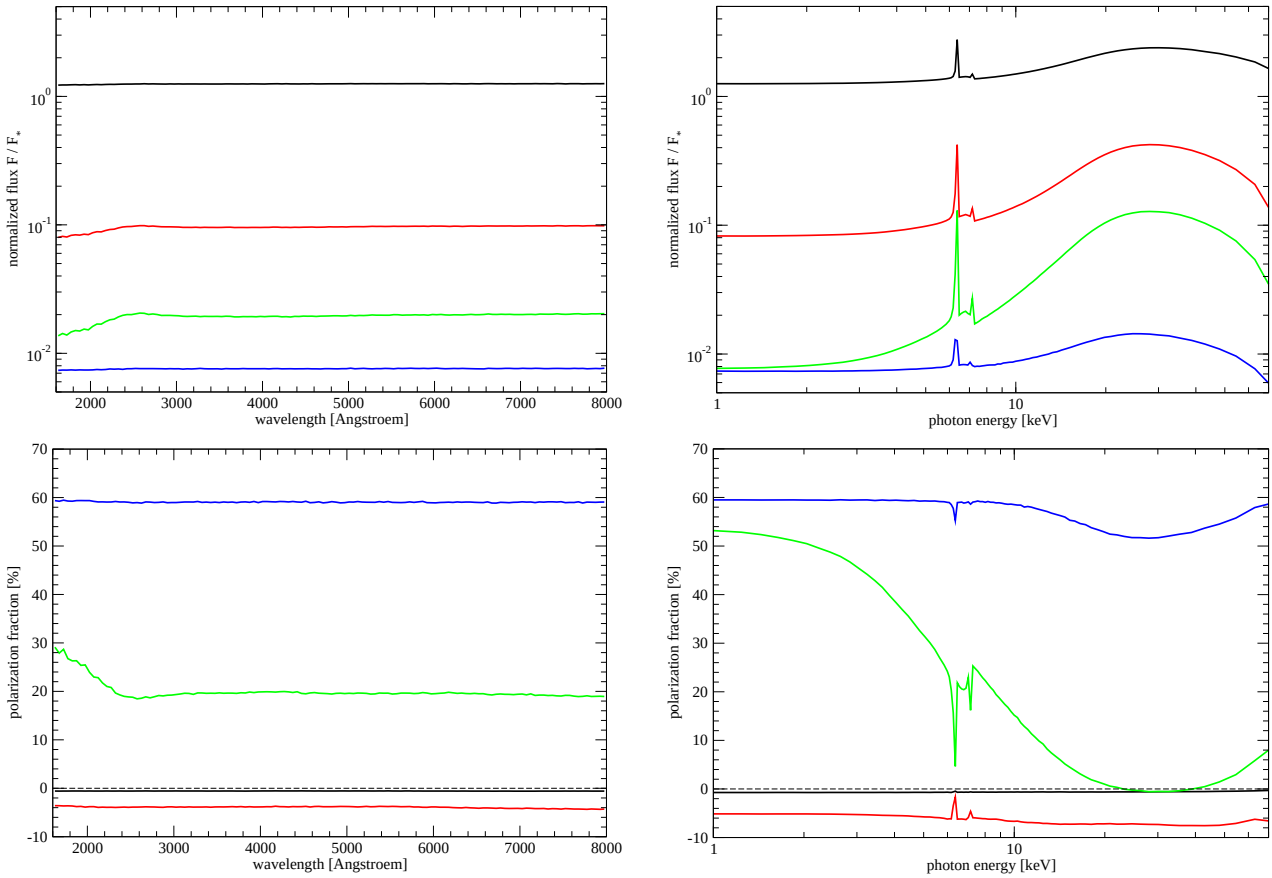

Fig. 1. Modeling the radiative coupling between the different axis-symmetric reprocessing regions. The normalized spectral flux is shown in the top panels, the polarization properties are shown below. A negative P denotes a "type-1" polarization (parallel to the projected symmetry axis) and a positive P stands for a "type-2" polarization (perpendicular to the axis). The transition at $P = 0$ is indicated by dashed lines. Four different viewing angles, i, are considered: a face-on view at $i \sim 18°$ (black), a line-of-sight just below the torus horizon at $\cos i = 0.63°$ (red), an intermediate type-2 view at $i \sim 76°$ (green), and an edge-on view at $i \sim 87°$ (blue). Left: optical/UV energy band. Right: X-ray band.

3 Results

In the top panels of Fig. 1, we present the total flux, F, for the two wavebands considered. The fluxes are normalized to the pure source flux, F_*, that would emerge along the same line-of-sight if there were no scattering media. The results for the polarization percentage, P, and for the polarization angle are combined in the bottom panels of Fig. 1. We adopt a sign convention for the polarization percentage that is recalled in the figure caption.

3.1 Results for the optical/UV band

At face-on and edge-on view, the optical flux is wavelength-independent indicating that electron-scattering in the equatorial flared-disk and in the polar outflows dominates. At intermediate viewing-angles, the impact of the wavelength-dependent dust scattering emerges, mostly around the λ_{2175} feature in the UV. This little bump at 2175 Å in the flux spectrum is due to scattering by carbonaceous dust in the torus.

The model reproduces the observed polarization dichotomy. The signature of the flared-disk is visible exceeding the effects of the polar outflow and producing low degrees of parallel polarization towards face-on viewing angles. At higher inclination, the equatorial scattering is hidden by the dusty torus and polar scattering dominates causing perpendicular polarization. The variations of P with wavelength at intermediate viewing angles indicate that the dusty torus also has a significant impact on the polarization. The rise in P towards the UV at $i \sim 73°$ is a combined effect of multiple scattering inside the torus funnel and of the wavelength-dependent polarization phase function that is associated with Mie scattering by Galactic dust.

3.2 Results for the X-ray band

The X-ray spectrum shows typical features of neutral reprocessing – the iron Kα and Kβ fluorescence lines at 6.4 keV and 7.1 keV and their absorption edges, the Compton hump, and strong soft X-ray absorption at intermediate viewing angles are prominent spectral features. The fluorescent line emission and the Compton reflection hump around 30 keV are present at every line of sight.

An important result of our modeling is that we predict a polarization dichotomy also for the X-ray band. At all viewing directions below the torus horizon, P is positive implying perpendicular polarization. But towards a face-on view, the electron scattering in the equatorial flared disk predominates and produces a net parallel polarization. A peculiar feature appears at $i \sim 73°$, where P changes from positive to mildly negative values around the Compton hump. This behavior is due to the competition between parallel and perpendicular polarization emerging from different reprocessing regions of the model. Around 30 keV, the effect of the flared disk becomes less important than the Compton scattering in the other regions. Explaining this behavior in detail is not trivial as several factors have to be taken into account, one of them being the angle-dependent scattering phase function. But also,the energy-dependence of the electron scattering cross-section has an effect as it favors soft X-ray photons to scatter more than hard X-ray photons. Higher energy photons therefore pass more easily through the optically thin, equatorial scattering region without interacting. This partly explains the disappearance of the parallel polarization at higher photon energy. A more detailed discussion about the X-ray polarization signature of isolated and coupled reprocessing regions is going to be provided elsewhere.

4 Summary and conclusions

We have applied the latest version of the STOKES radiative transfer code to examine the complex reprocessing between different, axis-symmetric media of an active nucleus. We provide simultaneous results for the optical/UV and for the X-ray wavebands and we trace the spectral flux and the polarization as a function of photon wavelength. The observed optical/UV polarization dichotomy is successfully reproduced and an analogous dichotomy is predicted for the X-ray range.

This work is carried out in anticipation of the forthcoming age of X-ray polarimetry. The NASA space telescope GEMS (Kallman et al. 2010) is planned to be launched in 2014 and will be entirely dedicated to X-ray polarimetry. The satellite will observe X-ray sources in the 2–10 keV band allowing us to test the soft X-ray part of our modeling results for the brightest AGN. Note that a next generation, broad-band X-ray polarimeter is technically feasible (Tagliaferri et al. 2011) and could even observe polarization up to 35 keV. Such observations include the X-ray polarization of the Compton hump and thus put even stronger constraints on the validity of our modeling results.

The authors are grateful to Martin Gaskell at the University of Valparaíso in Chile for his great help.

References

Angel, J. R. P. 1969, ApJ, 158, 219

Antonucci, R. 1993, ARA&A, 31, 473

Antonucci, R. R. J. 1983, Nature, 303, 158

Antonucci, R. R. J. 1984, ApJ, 281, 112

Chandrasekhar, S. 1960, Radiative transfer, ed. S. Chandrasekhar

Fath, E. A. 1909, Popular Astronomy, 17, 504

Goosmann, R. W. & Gaskell, C. M. 2007, A&A, 465, 129

Goosmann, R. W. & Matt, G. 2011, MNRAS, 415, 3119

Henney, W. J. & Axon, D. J. 1995, ApJ, 454, 233

Kallman, T. R., Swank, J. H., & GEMS Team. 2010, in Bulletin of the American Astronomical Society, Vol. 42, AAS/High Energy Astrophysics Division #11, 737–+

Kartje, J. F. 1995, ApJ, 452, 565

Smith, J. E., Robinson, A., Alexander, D. M., et al. 2004, MNRAS, 350, 140

Sunyaev, R. A. & Titarchuk, L. G. 1985, A&A, 143, 374

Tagliaferri, G., Hornstrup, A., Huovelin, J., et al. 2011, Experimental Astronomy, 98

Urry, C. M. & Padovani, P. 1995, PASP, 107, 803

Wolf, S. & Henning, T. 1999, A&A, 341, 675